International Journal of Computing and Digital Systems

Radial Lens Distortion Calibration from Spheres: Theory and Method

Moumen T. El-Melegy

Electrical Engineering Department, Assiut University, Assiut 71516, Egypt
e-mail: moumen@aun.edu.eg

Received 31 Aug. 2012, Revised 3 Nov. 2012, Accepted 10 Dec. 2012

Abstract: This paper addresses the problem of lens distortion calibration from a single image of a sphere. Almost all calibration methods based on spheres have focused on estimating all the camera parameters except the lens distortion ones which are left for another independent calibration process not using spheres. The paper presents for the first time a radial lens distortion calibration method based on the analysis of local shading measures in the sphere image. Several properties of these measures are pointed out and validated. While these measures are robust to noise, they are shown to vary nonlinearly as a function of lens distortion. As such, they can work as a basis for lens distortion calibration. The proposed method is easy to use and requires no specific feature extraction from the images. Experiments on simulated and real data are reported with comparisons to well-known techniques.

Keywords: lens distortion, camera calibration, image formation, local shading analysis**.**

I. INTRODUCTION

Camera calibration is an important component of any vision task which seeks to extract geometric information from a scene. It consists of finding the mapping between the 3D space and the camera plane. This modeling requires the determination of several camera parameters, including its position and orientation in space (extrinsic parameters), the image center, and lens focal length (intrinsic parameters). This distortion-free camera model simplifies a lot of considerations on geometry in which cameras are involved. However, for some applications which require high accuracy, or in cases where low-cost or wide-angle lens are used, these parameters are not sufficient and more parameters should be estimated to take into account camera lens distortion.

Up to now, a variety of methods for lens distortion calibration have been developed to accommodate various applications. These methods exhibit a trade-off between geometric accuracy and flexibility. Classical calibration techniques use a highly accurate tailor-made 3D calibration grid to estimate the lens distortion parameters along with the (extrinsic and intrinsic) parameters of the camera model [22, 24, 28]. These methods can achieve high calibration accuracy, but are less flexible and easier to use. Some more recent, less-demanding methods make use of 2D grids to calibrate only lens distortion parameters [12, 23, 29, 33]. Several other non-metric methods do not rely on known scene points or need calibration objects of known structure. These methods thus seek more flexibility of use at the possible expense of less accuracy or stability of results. The majority of such methods rely on the presence of straight lines in the scene [3, 5, 17, 21, 7, 8, 4, 32]. However they need some user guidance to localize these lines. Similarly, the method of Becker and Dove [2] requires the manual grouping of three mutually orthogonal sets of parallel lines and then the minimum vanishing point dispersion constraint to recover distortion parameters. Other methods use correspondences between points in different images from multiple views to compute camera distortion parameters [20, 10]. Correspondence can be established manually or automatically. However establishing correspondence automatically is rather not easy to solve and is likely to produce some false data to the calibration algorithm. Texture has also been utilized for lens distortion calibration [30]. The technique of blind removal of lens distortion based on polyspectral analysis [9] represents the extreme of calibration flexibility, but works where only qualitative (less-accurate) results are required.

The use of spheres in camera calibration dates back to 1991, when Penna [15] presented a simple method for recovering the aspect ratio of the two image axes from an image of a sphere. Due to their complete symmetry, spheres are attractive as a calibration pattern. Their silhouette is always visible by a camera in any arbitrary orientation provided that the sphere is inside the field of view of the camera. This justifies the increasing number of calibration methods based on spheres (e.g., [25, 26, 31]) especially for calibrating multiple camera systems. However almost all these methods have focused on estimating the camera parameters except the lens distortion ones which are presumably left for another independent calibration process not using spheres.

This paper investigates solving the problem of lens distortion calibration using a single image of a sphere under uniform illumination. To the best of our knowledge, this has not been addressed before in literature. We focus here on recovering the radial component of lens distortion, as it is often the most prominent in images [13, 11]. To tackle this problem, we pursue a non-traditional approach in the context of the calibration from spheres. For example, the occluding

contour of the sphere and its relationship to the absolute conic are not employed. Instead, we examine the mathematical model of the process of image shading formation of a sphere. This is typically done within the classical framework of Shape from Shading (SFS) [13]. Our approach is based on local shading measures derived under typical SFS assumptions. We go further with the analysis of image shading beyond the works by Pentland [16], Zheng and Chellappa [27], and Lee and Rosenfeld [14]. All these previous efforts used some local shading measures to estimate the light source direction as a pre-requisite step needed for subsequent SFS recovery algorithms. We derive a set of measures that are function of the second order derivatives of the image intensity values. These measures have a number of interesting properties, such as invariance to linear transformation of image intensities, albedo changes across the image, and to the light source direction. While these measures are shown to be robust to noise, they deviate nonlinearly from their theoretical average values as a function of lens distortion. We thus show that it is indeed possible, both theoretically and practically, to calibrate lens distortion using an image of a sphere. All that is required by this new calibration method is an image of a sphere, with no user intervention required at all. Accordingly this method can be a very easy and flexible way to calibrate and remove lens distortion of a camera.

The rest of the paper is organized as follows. Section II studies the image formation process for a sphere and derives some local shading measures. Implementation issues and noise sensitivity are also analyzed. In Section III, we propose a new algorithm to calibrate radial lens distortion. Section IV describes several experiments to evaluate our method. Finally, a record of our conclusions and future work is given in Section V.

II. SPHERE-BASED LOCAL SHADING MEASURES

Let assume that a sphere placed in front of the camera is parameterized as:

$$\begin{aligned} X &= a + r\sin\beta\cos\alpha, \\ Y &= b + r\sin\beta\sin\alpha, \\ Z &= c + r\cos\beta, \end{aligned} \tag{1}$$

where (X,Y,Z) is a 3D point on the sphere whose center is (c,b,c) and radius r. $\alpha = \alpha(X,Y,Z)$ and $\beta = \beta(X,Y,Y)$ represent the tilt and slant angles, respectively, of the surface normal of the sphere at this 3D point. Assuming a Lambertian surface of the sphere, the intensity $I(x,y)$ at any (x,y) point in an image of this sphere is given by [13]

$$I(x,y) = \eta\vec{N}.\vec{L} + \mu, \tag{2}$$

where η is the surface albedo, $\vec{N} = (\cos\alpha\sin\beta, \sin\alpha\sin\beta, \cos\beta)$ is the surface normal at the 3D point (X,Y,Z), while $\vec{L}$ is the unit vector for the illuminant direction, which can be parameterized such that $\vec{L} = (\cos\tau\sin\gamma, \sin\tau\sin\gamma, \cos\gamma)$, where τ is the tilt angle and γ is the slant angle. The last equation term, μ, is an ambient lighting term. We exclude the presence of interreflections among surface patches.

An image point (x,y) is related to its corresponding 3D point (X,Y,Z) via the perspective projection equations [11, 13]. However if the depth variation of the surface is small compared with its distance to the camera, then the perspective projection can be well approximated by *weak perspective projection* [1]. Following this assumption with the Z axis parallel to the optical axis of the camera, the 3D-2D relationship is given by: $x = k\,X / Z_0, y = k\,Y / Z_0$, where Z_0 is the average depth of the 3D surface, and k is a scale factor (related to camera focal length). Note that in typical SFS formulation the projection is assumed orthographic (i.e., $x = X, y = Y$), which we improve on in this work.

Using these representations, (2) becomes

$$\begin{aligned} I(x,y) = \eta(&\cos\tau\sin\gamma\cos\alpha\sin\beta + \\ &\sin\tau\sin\gamma\sin\alpha\sin\beta + \cos\gamma\cos\beta). \end{aligned} \tag{3}$$

After some computation, the image derivative I_x at a point (x,y) can be found as:

$$\begin{aligned} I_x &= \frac{\partial I}{\partial x} = \frac{\partial I}{\partial \alpha}\frac{\partial \alpha}{\partial x} + \frac{\partial I}{\partial \beta}\frac{\partial \beta}{\partial x} \\ &= \frac{\eta Z_0}{k\,r}(\sin\gamma\sin\beta\sin(\alpha-\tau)\frac{\sin\alpha}{\sin\beta} \\ &\quad +[\sin\gamma\cos\beta\cos(\alpha-\tau) - \cos\gamma\sin\beta]\frac{\cos\alpha}{\cos\beta}) \\ &= \frac{\eta Z_0}{k\,r}(\cos\tau\sin\gamma - \cos\gamma\tan\beta\cos\alpha). \end{aligned} \tag{4}$$

Similarly,

$$I_y = \frac{\partial I}{\partial y} = \frac{\eta Z_0}{r\,k}(\sin\tau\sin\gamma - \cos\gamma\tan\beta\sin\alpha),$$

$$I_{xx} = \frac{\partial I_x}{\partial x} = -\frac{Z_0^2\eta\cos\gamma}{k^2\,r^2\cos^3\beta}(\sin^2\alpha\cos^2\beta + \cos^2\alpha),$$

$$I_{yy} = \frac{\partial I_y}{\partial y} = -\frac{Z_0^2\eta\cos\gamma}{k^2\,r^2\cos^3\beta}(\cos^2\alpha\cos^2\beta + \sin^2\alpha),$$

$$I_{xy} = \frac{\partial I_x}{\partial y} = \frac{Z_0^2\eta\cos\gamma\sin 2\alpha}{2k^2\,r^2\cos^3\beta}(\cos^2\beta - 1), \text{ and}$$

$$\nabla^2 I = I_{xx} + I_{yy} = -\frac{Z_0^2\eta\cos\gamma}{k^2\,r^2\cos^3\beta}(\cos^2\beta + 1). \tag{5}$$

These derived quantities are then normalized by the image Laplacian $\nabla^2 I$ leading to the following ratios at any image point (x,y):

$$\begin{aligned} i_{xx} &= \frac{I_{xx}}{\nabla^2 I} = \frac{\sin^2\alpha\cos^2\beta + \cos^2\alpha}{\cos^2\beta + 1}, \\ i_{yy} &= \frac{I_{yy}}{\nabla^2 I} = \frac{\cos^2\alpha\cos^2\beta + \sin^2\alpha}{\cos^2\beta + 1}, \\ i_{xy} &= \frac{I_{xy}}{\nabla^2 I} = \frac{\sin 2\alpha(1-\cos^2\beta)}{2(\cos^2\beta + 1)}. \end{aligned} \tag{6}$$

A careful examination of these derived ratios of (6) reveals several interesting properties. They depend only on the tilt and slant angles of the surface normal at any point. However they do not depend on the illuminant direction, ambient lighting, the radius and center of the sphere, the reference depth plane

Z_0 of the weak-perspective projection or the camera scale (or focal length) k. More importantly, the dependency on the surface albedo is eliminated. Thus it does not matter whether the albedo is uniform or varying throughout the surface points. They are also invariant to linear transformation of the image intensity. For example, scaling and/or shifting the image intensities will not affect them. One last clear observation, $i_{xx} + i_{yy} = 1$ for any point.

If the statistical distributions of α and β are known, one can obtain the theoretical expected values of these local measures throughout the whole image. Such distributions can be easily derived for a sphere. The distributions f_α and f_β of α and β, respectively, are obtained as [27]

$$f_\alpha = \frac{1}{2\pi}, 0 \le \alpha < 2\pi; \; f_\beta = \cos\beta, 0 \le \beta \le \pi/2. \quad (7)$$

As such, the expected value of i_{xx} is given by:

$$\overline{I_{xx}} = \mathrm{E}\{i_{xx}\} = \frac{1}{2\pi}\int_{\alpha=0}^{2\pi}\int_{\beta=0}^{\pi/2} i_{xx}\cos\beta \, d\alpha \, d\beta = 0.5. \quad (8)$$

Similarly, $\overline{I_{yy}} = \mathrm{E}\{i_{yy}\} = 0.5$, and $\overline{I_{xy}} = \mathrm{E}\{i_{xy}\} = 0$. In simple words, the theoretical average values of the local shading measures i_{xx} and i_{yy} are 0.5, while that of the local measure i_{xy} is 0.

The expected values of these local measures are *practically* estimated from the images using the arithmetic means. In common practice, the derivatives of a Gaussian function are employed to compute the derivatives of a sampled image function via convolution [18]. This way, differentiation is combined with smoothing. The 2D zero mean Gaussian is defined as [18]

$$G = \frac{1}{2\pi\sigma^2}\exp\left(-\frac{x^2+y^2}{2\sigma^2}\right). \quad (9)$$

The second order partial derivative are $G_{xx} = (x^2 - \sigma^2)/\sigma^4 \, G$, $G_{yy} = (y^2 - \sigma^2)/\sigma^4 \, G$, and $G_{xy} = x\,y/\sigma^4 \, G$. A larger σ produces better noise suppression but, at the same time, distorts the signal more, and vice versa. In our implementation, we used $\sigma = 0.5$ and kernel size 5×5. With these kernels, $\overline{I_{xx}}$, for example, is implemented for an image I as

$$\overline{I_{xx}} = \frac{1}{size(I)}\sum_{x\varepsilon I}\sum_{y\varepsilon I}\frac{I \otimes G_{xx}}{I \otimes G_{xx} + I \otimes G_{yy}}, \quad (10)$$

where $\otimes$ denotes convolution. The summation is done on all image points belonging to the surface image, but points with zero Laplacian (zero denominator in (10)) are discarded. It is also important to point out that a more robust estimate of the means of these local measures can be obtained by replacing the arithmetic mean in (10)) by the median function.

Validation. To validate these local measures and their arithmetic means (10), a set of one hundred real and synthetic images for spheres are harvested from the Internet (mainly using Google Image Search); several examples are shown in Figure 1. The sphere images in these images are segmented out manually (and thus the backgrounds are removed), and converted to gray-scale images. Then the local shading measures are computed. The mean, standard deviation and median of each local measures, computed over all the collection of images, are listed in Table 1. Clearly, in spite of the variations of the spheres' colors and textures, the tabulated results show that the computed values are nearly as expected: $\overline{I_{xx}} \approx 0.5$, $\overline{I_{yy}} \approx 0.5$ and $\overline{I_{xy}} \approx 0$.

Figure 1. Sample validation sphere images harvested from the Internet.

TABLE 1: STATISTICS OF LOCAL SHADING MEASURES.

	mean	**std**	**median**
$\overline{I_{xx}}$	0.4978	0.0579	0.4911
$\overline{I_{yy}}$	0.5022	0.0579	0.5089
$\overline{I_{xy}}$	0.0086	0.0291	0.0020

Noise sensitivity. Due to image noise, there may be some fluctuations in the estimations of I_{xx}, I_{yy} and I_{xy}. This would lead to fluctuations in the estimated averages of the local shading measures. However using the way described above to compute the local shading means, one can show, both theoretically and experimentally, that these means have rather small noise sensitivity. To demonstrate this, the sphere image in Figure 2(a)) is corrupted with zero-mean Gaussian noise with standard deviation σ'. The arithmetic averages of the local measures are computed for different noise levels up to $\sigma' = 50$ in steps of 5, repeated 10 times per noise level. The averaged variations as a function of σ' are shown in Figure 2(b). The figure shows a predominantly stable performance of the three measures even at high noise levels.

III. LENS DISTORTION CALIBRATION ALGORITHM

In this section, we use the derived local shading measures and their expected values to develop an easy method to calibrate the camera's radial lens distortion. The measures are invariant under linear transformation of image intensity values. However, common imaging non-linearities, such as lens distortion, give rise to deviations in the computed local measures. To see this, consider the standard model for the radial lens distortion [11, 19] that maps the observable distorted image coordinates, (x_d, y_d), to the physically unmeasurable, undistorted image coordinates, (x_u, y_u), according to the equation:

$$x_u = x_d + \kappa(x_d - c_x)[(x_d - c_x)^2 + (y_d - c_y)^2],$$
$$y_u = y_d + \kappa(y_d - c_y)[(x_d - c_x)^2 + (y_d - c_y)^2], \quad (11)$$

where κ is the radial distortion coefficient and (c_x, c_y) is the distortion center, often assumed at the image center [5, 7] (which we will follow in the sequel). Some researchers (e.g., [19, 24]) employ a higher-order lens distortion model with more coefficients than the one in (11) to account for lenses with severe distortion. However the common model in (11) is found sufficiently accurate in many practical cases [5, 11, 7, 4].

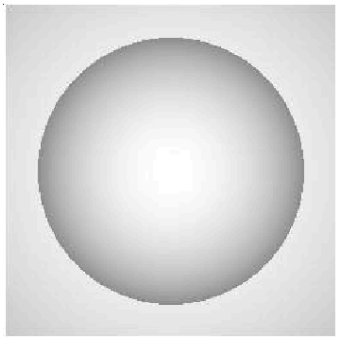

(a)

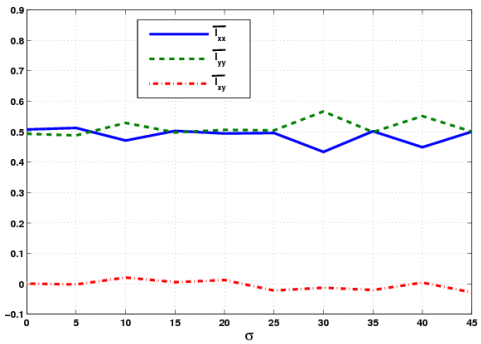

(b)

Figure 2: Noise sensitivity analysis: (a) A sample input image. (b) The arithmetic averages of the three measures versus different noise levels in the sphere image.

Now if an image, like the one shown in Figure 2(a)), is subjected to various amounts of radial distortion controlled by different values of κ in the big distortion range of $-10\times10^{-6} \le \kappa \le 10\times10^{-6}$, the computed means of the local shading measures will, expectedly, deviate from their theoretical no-distortion values in (8) as κ moves away from zero, see Figure 3(a)-(c). To assess how much these measures are far from the distortion-free case, the following error is proposed

$$\varepsilon_\kappa = |\overline{I_{xx}}(U_\kappa(I)) - 0.5| + |\overline{I_{xy}}(U_\kappa(I))|, \quad (12)$$

where $\overline{I_{xx}}(U_\kappa(I))$ denotes the mean of the shading measure computed for the image after being undistorted via the mapping U_κ in (11) at κ. In principle, this error estimates how much the means of the local shading measures i_{xx} and i_{xy} for the undistorted image are far from their theoretical value (0.5 and 0 , respectively). For a properly undistorted image, the averages of these local shading measures will be close to their theoretical values rendering the error ε_κ significantly small (ideally zero). Note that $\overline{I_{yy}}$ is not utilized (nor needed) in (12) as the two shading measures $\overline{I_{xx}}$ and $\overline{I_{yy}}$ are related (thus not independent).

Figure 3(d) plots the error ε_κ as a function of κ for the distortion-free image in Figure 2(a)). The error shows here several local minima, but the global minimum is still at the correct value of κ (zero for this distortion-free image).

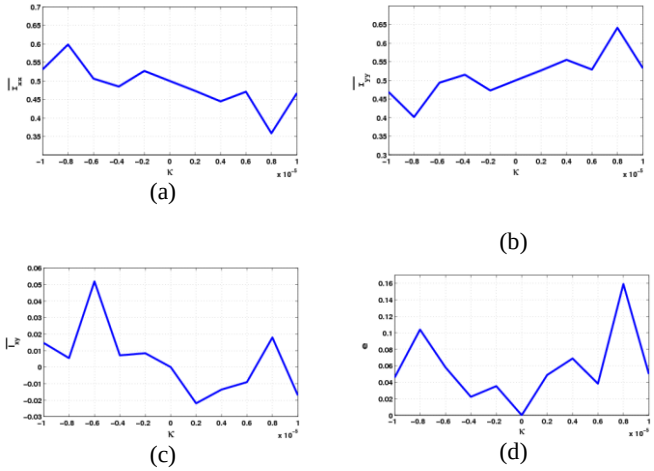

(a) (b) (c) (d)

Figure 3: Effect of lens distortion on means of local shading measures: (a) $\overline{I_{xx}}$, (b) $\overline{I_{yy}}$ (c) $\overline{I_{xy}}$, (d) Error ε_κ versus κ.

Following this idea we can devise a easy procedure to calibrate the radial lens distortion coefficient for a given camera: Capture an image by that camera for a ball with a surface, which can be assumed Lambertian, under constant distribution of illumination. According to the mean value theorem, any constant distribution of illumination is equivalent to a single distant point-source illuminant [16]. If the camera is placed at a rather large distance compared to the sphere radius, the weak perspective projection can also be reasonably assumed. At this point, the deviation of the image intrinsics off their theoretical values is presumably attributed to lens geometric distortion.

It is then required to find the radial distortion coefficient κ in the distortion model (11) that will drive the local shading measures of the image undistorted by U_κ closer to their theoretical average values, thus minimizing the error in (12).

To solve this nonlinear optimization problem, some care must be taken. Since the error ε_κ often has several local minima (please refer to Figure 3(d)), relying on pure gradient-based minimization routines will not have much luck in finding the optimal solution due to being trapped in local minima. We therefore resort to a global optimization routine, such as simulated annealing starting from the initial point $\kappa = 0$, in order to solve this nonlinear optimization problem in one variable.

The simulated annealing routine requires many evaluations of the objective error in (12) at the various attempted values of κ. One such evaluation would require the whole input image be undistorted first using the attempted κ, and then the

shading measures and their averages are to be computed from the undistorted image. However significant speedup can be attained by avoiding the computationally expensive operation of undistorting the whole input image before computing the shading measures. This can be done by relating the first and second image derivatives of the unknown undistorted image to the derivatives of the given distorted image as a function of κ, see Appendix. This way, the local shading measures for the undistorted image (and thus the error ε_κ at a particular κ) can be computed from those obtained image derivatives without having to undistort the input image first.

Once the distortion model coefficient for a particular camera has been estimated, any images captured by this camera can be easily undistorted. Note that the above calibration procedure can be used if the image captured by the camera includes one or more balls. The latter case of having multiple balls in the captured image is in practice more desirable as it allows the balls to occupy more of the image spatial domain thus capturing more from the distortion effect introduced in the image, without the need to use larger balls. In the same time, this helps satisfy the required condition between the ball-to-camera distance and the ball diameter, which is needed for the weak perspective projection assumption.

IV. EXPERIMENTAL RESULTS

The calibration method is evaluated using simulations as well as experiments with real data to calibrate the lens distortion of two cameras. The proposed method is compared with two popular methods in the literature, namely the well-known line straightness based method [5] and a differential approach for lens distortion calibration [7].

A. Simulations

An experiment with simulated data is carried out to quantify the accuracy of the proposed method versus various noise levels noise. Since the existing methods under comparison [5, 7] require different input data, no comparative results are obtained for this experiment.

A synthetic image of size 1024×1024 for a textureless sphere has been generated, see Figure 4(a). The image is then distorted with a number of different radial distortion coefficients (1×10^{-6}, 5×10^{-6}, and 9×10^{-6}). For each distortion degree, the distorted image is afterwards corrupted with Gaussian noise of zero mean and standard deviation in the range of 0 to 20. At each value of noise standard deviation, the proposed method is applied to estimate the lens distortion coefficient. The same procedure is repeated 10 times and the average estimated distortion coefficient is plotted in Figure 4(b) versus the noise standard deviation. The figure clearly shows a predominantly accurate performance of the proposed method versus noise. The estimated distortion coefficient is consistently close to the ground-truth value even at high noise levels.

To test the proposed method performance on textured surfaces, the whole above experiment is repeated for a textured sphere image, see Figure 5(a). The image is also distorted with the same three values for the radial distortion coefficient, and the Gaussian noise standard deviation is varied in the range of 0 to 20. The average distortion coefficient estimated by the proposed method is plotted in Figure 5(b) versus the noise standard deviation for the three ground truth values. Again the estimated distortion coefficients are consistently close to the ground-truth values even at high noise levels.

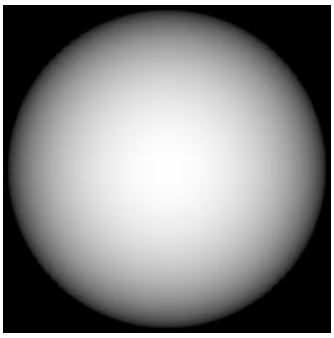

(a)

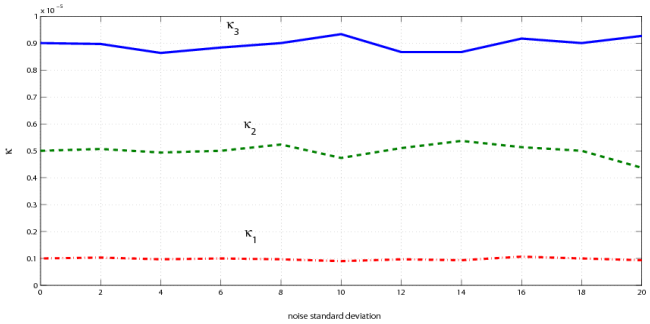

(b)

Figure 4: Proposed method performance versus noise: (a) Input synthetic sphere image. (b) The estimated lens distortion coefficient κ versus noise standard deviation for 3 ground truth values (1×10^{-6}, 5×10^{-6}, and 9×10^{-6}).

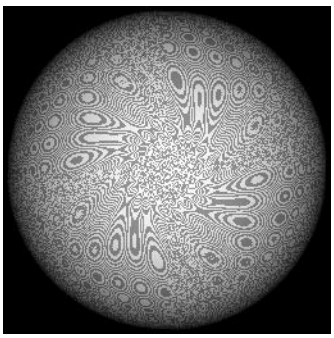

(a)

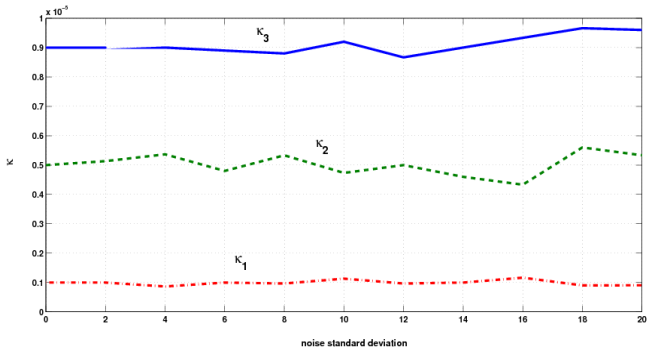

(b)

Figure 5: Proposed method performance versus noise: (a) Input synthetic textured sphere image. (b) The estimated lens distortion coefficient κ versus noise standard deviation for 3 ground truth values (1×10^{-6}, 5×10^{-6}, and 9×10^{-6}).

B. Real Experiment I

The proposed method is then experimentally evaluated to calibrate the lens distortion for a cheap BenQ camera. Figure 6(a) shows an image acquired by that camera for a ball. In addition, two more images are taken by the same camera, one for a group of straight lines on a white paper, and another for a scene in our lab, see Figure 6(b) and (c). All acquired images are 320×240. Due to the low lens quality of this cheap camera, the images have noticeable lens distortion as evident from the small curvature of the images' supposed straight lines.

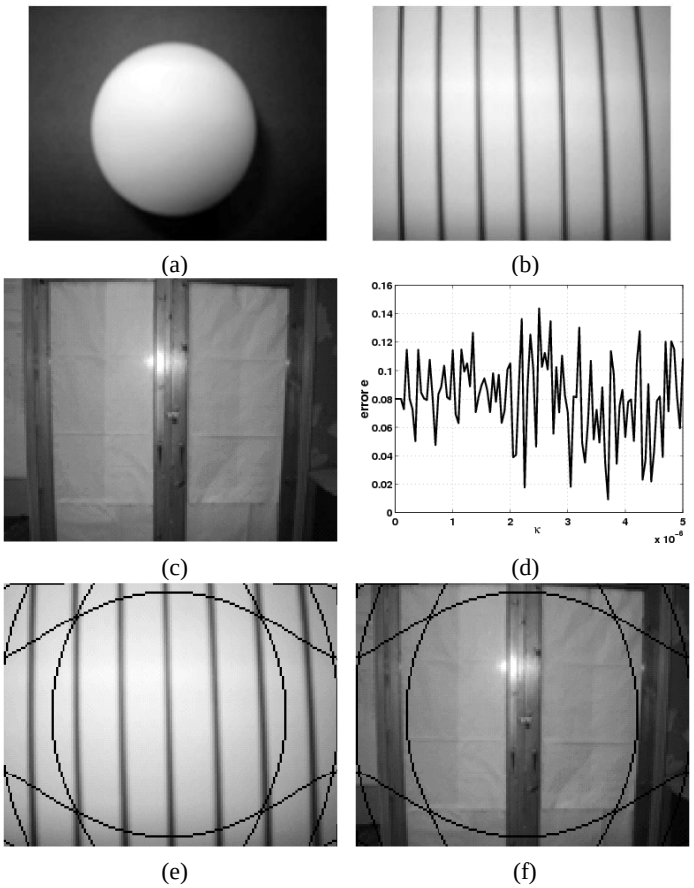

Figure 6: Lens distortion calibration: (a) Calibration image, (b) Image of straight lines on paper, (c) A real scene, (d) ε_κ versus κ, (e) Undistorted lines image, (f) Undistorted real scene.

The proposed method is applied to the image of the calibration ball, and the optimal value of the distortion coefficient is searched for over the range from 0 to 5×10^{-6}. For the sake of better visualization of the error being minimized, the objective error in (12) is plotted versus κ over this range in steps of 0.05×10^{-6} in Figure 6(d). The error clearly exhibits several local minima, which makes finding the global minimum of the error rather more difficult. The simulated annealing routine has estimated this global minimizer to be $\kappa = 3.7\times10^{-6}$. The run time is within 220s on a PC with 2.2GHz AMD processor and 4GB RAM. For the obtained κ, the camera images can be undistorted as shown in Figure 6(e) and (f). Clearly the lines have become fairly straighter in the corrected images, which reflects the good accuracy of the found distortion coefficient. Some circular artifacts are left on purpose on the undistorted image to demonstrate the inverse mapping of the distortion model, and to help visualize the differences between the original distorted images and the corrected ones. These artifacts can fairly removed, if desired, by doing some post-processing (as will be done in the following experiment).

The image of Figure 6(b) is also used to estimate the radial distortion coefficient by two well-known existing methods: the line straightness method [5] and a differential approach [7]. The results of these two methods as well as the proposed method are given in Table 2. The radial distortion coefficient found by the three methods are fairly close, and they give rise to virtually similar undistorted images. So it is rather hard to judge which method is more accurate. However the proposed method is easier and more flexible, with no user intervention required all. No specific features are needed to be reliably and accurately extracted from images. The other two methods need lines that should be straight to be accurately extracted from the image, and thus need some user guidance.

TABLE 2: REAL EXPERIMENT I COMPARISON.

Method	κ
Line straightness method [5]	3.00×10^{-6}
Differential method [7]	2.37×10^{-6}
Proposed method	3.70×10^{-6}

C. Real Experiment II

The proposed method is then used to calibrate lens distortion for a small-sized DiscoveryULTRA camera with a 2.0 mega pixel CCD imager. Figure 7(a) shows an image acquired by that camera for two ping-pong balls. Two balls are used here for calibration, not just one, to allow the balls to occupy more of the image spatial domain to capture more of the lens distortion effect without the need to use larger balls. In addition, another image is taken by the same camera for a group of straight lines on a white paper, see Figure 7(b). By looking at the images' lines, one can notice the evident lens distortion effect.

Applied to the two ball image, the proposed method has provided a value of $\kappa = 5.61\times10^{-6}$. The run time is within 140s on a PC with 2.2GHz AMD processor and 4GB RAM. For this value of κ, the camera images can be undistorted as shown in Figure 7(c). Clearly the lines have become indeed straighter in the corrected image. In this experiment, all artifacts resulting from the undistortion mapping are removed by 2D intensity interpolation. To test the method stability, another image for a larger ball is also captured, see Figure 7(d). Applied to this image, the method has yielded $\kappa = 5.59\times10^{-6}$, which is rather close to the previous estimate. As such, the proposed method is considerably stable.

The image of Figure 7(b) is also used to estimate the radial distortion coefficient by the two methods under comparison [5, 7]. The results are reported in Table 3. The radial distortion coefficient found by the three methods are again fairly close. While the two methods require precise localization of the lines' points and often under user's supervision, the proposed method works directly on the image of a sphere, without the need for specific features to be reliably extracted. As such, the proposed method is considered easier and more flexible with accuracy comparable to the other methods.

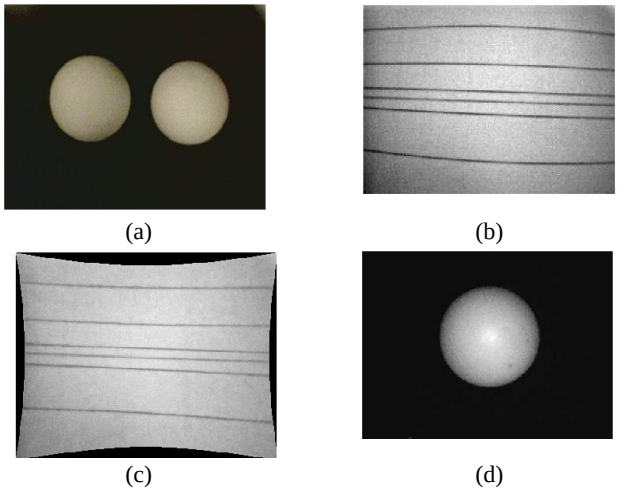

Figure 7: Lens distortion calibration: (a) Calibration image of two balls, (b) Image of straight lines on paper, (c) Undistorted lines image, (d) Another calibration image of one ball.

TABLE 3: REAL EXPERIMENT II COMPARISON.

Method	κ
Line straightness method [5]	5.81×10^{-6}
Differential method [7]	5.53×10^{-6}
Proposed method	5.61×10^{-6}

V. CONCLUSIONS AND FUTURE WORK

This paper has addressed the problem of lens distortion calibration from a single image of a sphere. To the best of our knowledge, this has not been addressed before in literature. We have shown that this is possible both in theory and practice. We have presented the first method in the literature for that sake.

Spheres have been found attractive for camera calibration [26, 25], especially in multiple camera systems, because of their complete symmetry and their ease to image by a camera in any arbitrary orientation (provided that the sphere is inside the field of view of the camera). However, all such methods have focused on estimating all the camera parameters except the lens distortion ones which are left for another independent calibration process not using spheres. As such, the proposed method can be useful to complement these methods.

Moreover, the paper has tackled this problem in a non-traditional approach in the context of the calibration from spheres as found in the literature (e.g., [25, 26, 31]). For example, the occluding contour of the sphere and its relationship to the absolute conic are not employed. Instead, the proposed method is built upon the analysis of the mathematical model of the image shading formation process in an image of a sphere and the derivation of some local shading measures. The paper has pointed out several properties of these measures, such as invariance to linear transformation of image intensities and to albedo changes across the image. These measures deviate nonlinearly away from their theoretical averages as a function of lens distortion. Thus they can work as a basis for lens distortion calibration. All that is required by this new calibration method is an image of one or more spheres under uniform illumination, with no user intervention required at all. Other than the simple segmentation of the sphere surface from the image, no specific features (e.g., corners or lines) are needed to be reliably and accurately extracted. Accordingly this method is an easy and flexible way to calibrate and remove a camera's lens distortion. It is also interesting to note that one can often find images of spheres in many every-day images. This opens the door to applying the proposed method to those images already captured with unknown cameras in order to estimate their lens distortion models.

The paper has presented several experiments to validate some properties of the developed measures. Simulations as well as experiments with real cameras have been reported to demonstrate the performance of the proposed calibration method. It it has provided comparable results to some well-known techniques [5, 7] that rely on specific and precise feature extraction.

It should be pointed out that there are certain limitations and restrictions to the proposed method. The method may suffer from the presence of shadows or specularities on the spheres. Furthermore, the sphere radius should be small compared with its distance to the camera. These are required to make the assumptions set forth in the derivation hold. However, these conditions are not very limiting to the applicability of the proposed method, keeping in mind the method's simplicity and ease-of-use. We are currently investigating relaxing some of these conditions (e.g., upgrading the weak perspective assumption to full perspective) to increase the method's applicability.

Another ongoing research direction is to generalize the findings of this work by investigating the question whether lens distortion can be calibrated from an image of any smooth surface, not just spheres. We have drafted some early answers to this question in a recent submission [6].

APPENDIX

The image derivatives needed to compute the shading measures for the unknown undistorted image $I^u(.,.)$ can be computed from the derivatives of the input distorted image $I^d(.,.)$ (to avoid the computationally expensive operation of undistorting the whole input image before computing the shading measures). This is given below in terms of the partial derivatives of the distorted image coordinates (x_d, y_d) with respect to the undistorted coordinates (x_u, y_u) . These derivatives can be computed from the distortion model (11).

$$I^u_x = I^d_x \frac{\partial x_d}{\partial x_u} + I^d_y \frac{\partial y_d}{\partial x_u} \tag{13}$$

$$I^u_y = I^d_x \frac{\partial x_d}{\partial y_u} + I^d_y \frac{\partial y_d}{\partial y_u} \tag{14}$$

$$I^u_{xx} = I^d_{xx}(\frac{\partial x_d}{\partial x_u})^2 + I^d_{xy}(\frac{\partial y_d}{\partial x_u}\frac{\partial x_d}{\partial x_u} + \frac{\partial x_d}{\partial x_u}\frac{\partial y_d}{\partial x_u}) + I^d_x \frac{\partial^2 x_d}{\partial x_u^2} + I^d_y \frac{\partial^2 y_d}{\partial x_u^2} + I^d_{yy}(\frac{\partial y_d}{\partial x_u})^2 \tag{15}$$

$$I^u_{yy} = I^d_{xx}(\frac{\partial x_d}{\partial y_u})^2 + I^d_{xy}(\frac{\partial x_d}{\partial y_u}\frac{\partial y_d}{\partial y_u} + \frac{\partial x_d}{\partial y_u}\frac{\partial y_d}{\partial y_u}) + I^d_x \frac{\partial^2 x_d}{\partial y_u^2} + I^d_y \frac{\partial^2 y_d}{\partial y_u^2} + I^d_{yy}(\frac{\partial y_d}{\partial y_u})^2 \tag{16}$$

$$I^u_{xy} = I^d_{xx}\frac{\partial x_d}{\partial y_u}\frac{\partial x_d}{\partial x_u} + I^d_{xy}\left(\frac{\partial y_d}{\partial y_u}\frac{\partial x_d}{\partial x_u} + \frac{\partial x_d}{\partial y_u}\frac{\partial y_d}{\partial x_u}\right) + I^d_x\frac{\partial^2 x_d}{\partial y_u \partial x_u} + I^d_y\frac{\partial^2 y_d}{\partial y_u \partial x_u} + I^d_{yy}\frac{\partial y_d}{\partial y_u}\frac{\partial y_d}{\partial x_u} \quad (17)$$

REFERENCES

[1] J. Aloimonos, "Perspective approximations," *Image and Vision Computing*, Vol. 8(3), pp. 179 – 192, 1990.

[2] S. Becker and V. Bove, "Semi-automatic 3d model extraction from uncalibrated 2d camera views," *Proc. SPIE Visual Data Exploration and Analysis II*, Vol. 2, Feb. 1995, pp. 447–461.

[3] D.C. Brown, "Close-range camera calibration," *Phtogrammetric Engineering*, Vol. 37(8), pp. 855–866, Aug 1971.

[4] Faisal Bukhari and Matthew Dailey, "Robust radial distortion from a single image," in *Advances in Visual Computing*, George Bebis, Richard Boyle, Bahram Parvin, Darko Koracin, Ronald Chung, Riad Hammound, Muhammad Hussain, Tan Kar-Han, Roger Crawfis, Daniel Thalmann, David Kao, and Lisa Avila, Eds., vol. 6454 of *Lecture Notes in Computer Science*, pp. 11–20. Springer Berlin / Heidelberg, 2010.

[5] F. Devernay and O. Faugeras, "Straight lines have to be straight: Automatic calibration and removal of distortion from scenes of structured environments," *Machine Vision and Applications*, Vol. 1, pp. 14–24, 2001.

[6] Moumen El-Melegy and Aly A. Farag, "Can lens distortion be calibrated from an image of a smooth, textureless lambertian surface?" in *Proc. IEEE International Conference on Image Processing (ICIP)*, Florida, USA, Sept. 30 - Oct. 3, 2012.

[7] M. Ahmed and A. Farag, "Nonmetric calibration of camera lens distortion: differential methods and robust estimation," *IEEE Transactions on Image Processing*, Vol. 14, No. 8, pp. 1215 –1230, 2005.

[8] Moumen T. El-Melegy and Nagi H. Al-Ashwal, "Lens distortion calibration using level sets," in *Variational, Geometric, and Level Set Methods in Computer Vision (VLSM'05)*, N. Paragios, O. Faugeras, and T. Chan, and C. Schnörr, Eds, Vol. 3752, Lecture Notes in Computer Science, Springer Berlin/Heidelberg, pp. 356-367, 2005.

[9] Hany Farid and Alin C. Popescu, "Blind removal of image non-linearities," in *Proc. IEEE International Conference on Computer Vision (ICCV)*, Vancouver, BC, Canada, Vol. 1, pp. 76 –81, 2001.

[10] A. W. Fitzgibbon, "Simultaneous linear estimation of multiple view geometry and lens distortion," in *Proc. IEEE International Conference on Computer Vision and Pattern Recognition (CVPR)*, Kauai, HI, USA, 8-14 December 2001.

[11] R. Hartley and A. Zisserman, *Multiple view geometry in computer vision*, 2nd Edition, Cambridge University Press, 2004.

[12] R. Hartley and S.B. Kang, "Parameter-free radial distortion correction with centre of distortion estimation," in *Proceedings of the Tenth IEEE International Conference on Computer Vision*, 2005, pp. 1834–1841.

[13] B.K.P. Horn, *Robot Vision*, MIT Press, 1986.

[14] C. Lee and A. Rosenfeld, "Improved methods of estimating shape from shading using the light source coodinate system," *Artificial Intelligence*, Vol. 26, pp. 125–143, 1985.

[15] M.A. Penna, "Camera calibration: A quick and easy way to determine the scale factor," *IEEE Transactions on Pattern Analysis and Machine Intelligence (PAMI)*, Vol. 13, pp. 1240–1245, 1991.

[16] Alex P. Pentland, "Local shading analysis," *IEEE Transactions on Pattern Analysis and Machine Intelligence (PAMI)*, Vol. PAMI-6(2), pp. 170–187, 1984.

[17] B. Prescott and G. McLean, "Line-based correction of radial lens distortion," *Graphical Models and Image Processing*, Vol. 59(1), pp. 39–47, 1997.

[18] B. ter Haar Romeny, *Geometry-Driven Diffusion in Computer Vision*, Kluwer, 1994.

[19] C.C. Slama, *Manual of photogrammetry*, American Society of Photogrammetry, 1980.

[20] G.P. Stein, "Lens distortion calibration using point correspondences," in *Proc. IEEE Int. Conf. on computer Vision and Pattern Recognition*, San Francisco, June 1997, pp. 143–148.

[21] R. Swaminathan and S. Nayar, "Non-metric calibration of wide-angle lenses and polycameras," *IEEE Trans. on Pattern Analysis and Machine Intelligence (PAMI)*, Vol. 22(10), Oct. 2000.

[22] R. Tsai, "A versatile camera calibration technique for high-accuracy 3d machine vision metrology using off-the-shelf tv cameras and lenses," *IEEE J. of Robotics and Automation*, Vol. RA-3(4), pp. 1165–1172, Aug 1987.

[23] Carlos C. Ricolfe-Viala and A. Sánchez-Salmerón, "Robust metric calibration of non-linear camera lens distortion," *Pattern Recognition*, Vol. 43, pp. 1688–1699, April 2010.

[24] J. Weng, Paul Cohen, and M. Herniou, "Camera calibration with distortion models and accuracy evaluation," *IEEE Transactions on Pattern Analysis and Machine Intelligence (PAMI)*, Vol. 14(10), 1992.

[25] K.-Y.K. Wong, Guoqiang Zhang, and Zhihu Chen, "A stratified approach for camera calibration using spheres," *IEEE Transactions on Image Processing*, Vol. 20, No. 2, pp. 305 –316, 2011.

[26] H. Zhang, K.Y. Wong, and G. Zhang, "Camera calibration from images of spheres," *IEEE Transactions on Pattern Analysis and Machine Intelligence*, Vol. 29, No. 3, pp. 499 –502, 2007.

[27] Q. Zheng and R. Chellapa, "Estimation of illuminant direction, albedo and shape from shading," *IEEE Transactions on Pattern Analysis and Machine Intelligence (PAMI)*, Vol. 13(7), pp. 680–702, 1991.

[28] T. Rahman, and N. Krouglicof, "An efficient camera calibration technique offering robustness and accuracy over a wide range of lens distortion," *IEEE Transactions on Image Processing*, Vol.21(2), pp.626-637, 2012.

[29] L. Alvarez, L. Gómez, and P. Henríquez, "Zoom dependent lens distortion mathematical models," *Journal of Mathematical Imaging and Vision*, Springer Netherlands, Vol. 44(3), pp. 480-490, 2012.

[30] Z. Zhang, Y. Matsushita, and Y. Ma, "Camera calibration with lens distortion from low-rank textures," in *Proc. IEEE Conference on Computer Vision and Pattern Recognition (CVPR)*, Colorado Springs, CO, Vol. 1, pp.2321-2328, 2011.

[31] Z. Zhao and Y. Liu "Applications of projected circle centers in camera calibration," *Machine Vision and Applications*, Vol. 21(3), pp.301 - 307, 2010.

[32] E. Rosten, and R. Loveland, "Camera distortion self-calibration using the plumb-line constraint and minimal Hough entropy," *Machine Vision and Applications*, Vol. 22(1), pp. 77-85, 2011.

[33] C. Ricolfe-Viala, A. Sánchez-Salmerón, "Robust metric calibration of non-linear camera lens distortion," *Pattern Recognition*, Vol. 43(4), pp. 1688-1699, 2010.